Draft version October 4, 2022
Typeset using LaTeX **twocolumn** style in AASTeX631

Looking for the Largest Bound Atoms in Space

Corvus Koithan[1] and Pedro Salas[2]

[1] *Texas Tech University*
[2] *Green Bank Observatory*
Green Bank WV 24944

ABSTRACT

The largest bound atoms in space have extremely short lives, emitting radio recombination lines (RRLs) that enable the study of the physical conditions of the gas they are emitted from. This project studies hydrogen RRLs from the diffuse ionized gas in the W43 region using the high-frequency GBT Diffuse Ionized Gas Survey (GDIGS) and the first results from the GDIGS at Low frequencies (GDIGS-Low). We focus on the brightest emission in the data at around 100 $km\ s^{-1}$, and using a peak ratio model, compute density estimates on the order of 10 e^- cm^{-3}. We also detected Carbon RRLs, providing further avenues into studying cold atomic gas and the formation of molecular clouds.

1. INTRODUCTION

Radio recombination lines (RRLs) are emitted from atoms with high principal quantum numbers, called Rydberg atoms, which can be extremely large in diameter. These lines are extinction-free and can be brighter at low frequencies (<1 GHz) due to stimulated emission (Shaver 1975). Given their large diameter, the number of these atoms in a given energy level (level population) is extremely sensitive to the gas conditions such as density and the radiation field. Therefore, RRLs are great probes of the physical conditions of the gas they originate in. They offer a unique look into the interstellar medium (ISM), and the spectral lines contain kinematic information that is vital to this study.

Since the level population of the Rydberg atoms is sensitive to the physical conditions of the gas, we can use observations of RRLs at multiple frequencies (principal quantum numbers) to determine the gas density. Here, we make use of the GBT Diffuse Ionized Gas Survey (GDIGS) and GDIGS at Low frequencies (GDIGS-Low) surveys for this purpose. GDIGS observed RRLs using the C-band receiver on the GBT (4 to 7 GHz), while GDIGS-Low uses the prime focus receivers at 340 and 800 MHz. For more information on GDIGS, see Anderson et al. (2021).

We focus on the first data from GDIGS-Low in the region around the W43 star-forming complex, which contains a giant HII region; for more details, see Luong et al. (2011) and Motte et al. (2003). We mainly study hydrogen Hα lines from the diffuse ionized gas (DIG) in this area and note detected carbon emissions. This project aims to provide information on the physical properties of the diffuse ionized gas, specifically density. This can give details on the relationship between the DIG and HII regions and sources of ionization of the DIG, as well as how processes of stellar feedback, such as stellar winds, affect the DIG (Emig et al. 2020).

We discuss moment maps in Section 3 and moment comparison maps in 4. We analyze density estimates in 5, discuss carbon detection in 6, then conclude in 7.

2. METHODS

We use data from GDIGS and GDIGS-Low spanning about 30°<l<32°, b< |1|. GDIGS-Low is planned to consist of data at 340 and 800 MHz, but only 800 MHz data is used in this project. GDIGS is at about 5.7 GHz for the purposes of this project. The GDIGS-Low data is reduced via the GBT RRL pipeline [1]. GDIGS-Low has a spatial resolution of about 17' and GDIGS is at about 2' (Luisi et al. 2020). We smooth the GDIGS cubes to match the resolution of the GDIGS-Low cubes for comparison analyses. To this end, the GDIGS data is reprojected onto the GDIGS-Low data using the Python package *reproject* and a linear interpolation function. This reprojection is done twice as we were working on the data reduction during the project using newer data from GDIGS-Low; therefore, some maps in this report differ visually. The root mean squared noise per pixel (σ) of the cube is about 0.075 K. To avoid erroneous data during our analysis, we use a mask to ignore pixels which show emissions below the 3σ level.

[1] Data reduction pipeline used for GDIGS-Low data: https://github.com/astrofle/gbt-rrl-pipeline

3. MOMENT MAPS

In the GDIGS-Low data, we detect hydrogen RRL (HRRL) emissions at velocities of -60, 40, and 100 $km\ s^{-1}$. We focus on the velocity range of 60-140 $km\ s^{-1}$. We define this range to avoid the emission around 40 $km\ s^{-1}$ from affecting these maps as much as possible, as we want to focus on emission clearly associated with the W43 region we are studying (see Luisi et al. (2020) for details).

We create a moment 0 map (Fig. 1) which shows emission intensity integrated over the spectral channels according to the following equation, where M_0 represents moment 0, I is intensity, and v is velocity:

$$M_0 = \int I_v \, dv \tag{1}$$

Emissions extend from about $29.8^\circ < l < 32^\circ$, $-0.5^\circ < b < 0.3^\circ$ and are brightest with about 80 $K\ km\ s^{-1}$. They are more intense on the right side of the brightest emission, around 35 $K\ km\ s^{-1}$ compared to about 15 $K\ km\ s^{-1}$ on the left.

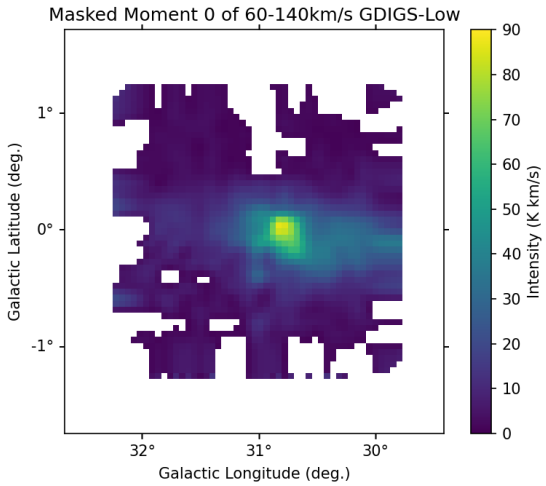

Figure 1. Moment 0 map of GDIGS-Low data showing integrated intensity of emissions. Emissions are brightest with about 80 $K\ km\ s^{-1}$ around 30.8° longitude and 0° latitude.

We then created a moment 1 map (Fig. 2) which shows radial velocity of the HRRL at about 100 $km\ s^{-1}$:

$$M_1 = \frac{\int v I_v \, dv}{\int I_v \, dv} \tag{2}$$

The central clump of gas around the same area of visible emissions from the moment 0 map is moving at about 100 $km\ s^{-1}$ throughout, which suggests that it is indeed a coherent clump of gas.

The last moment map is a full width at half maximum (FWHM) map (Fig. 3), also called a line width map,

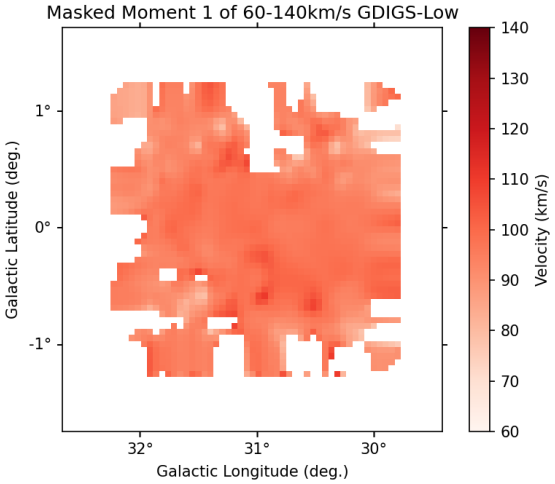

Figure 2. Moment 1 map of GDIGS-Low data showing radial velocity of gas.

which shows the width of the emission lines at half their peak in units of the spectral axis:

$$M_2 = \frac{\int I_v (v - M_1)^2 \, dv}{M_0} \tag{3}$$

We also see similar values in the general area of emissions as defined in the moment 0 map (Fig. 1), though there are more fluctuations. For comparison, Figure 4 has moment 0, 1, and FWHM maps of the GDIGS data. For more details on GDIGS in the W43 region, see Luisi et al. (2020).

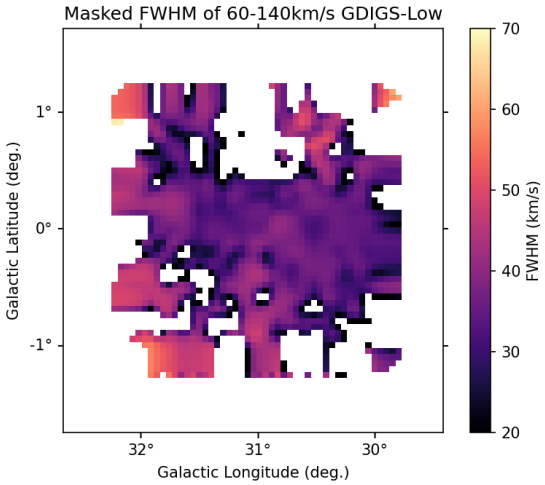

Figure 3. Full width half max map of GDIGS-Low data showing width of emissions.

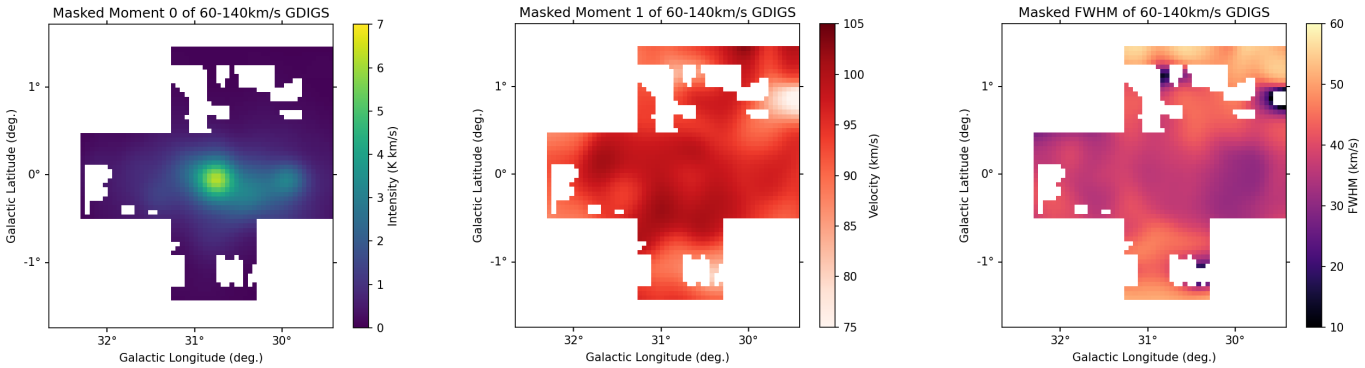

Figure 4. Moment maps of GDIGS data. Masked areas provide reference for location of GDIGS-Low data.

4. MOMENT COMPARISON MAPS

We compare the moment maps from GDIGS-Low to GDIGS moment maps computed similarly (Fig. 4). Only regions with data in both maps are shown in these comparison maps, hence the overall different shape.

The ratio moment 0 map (Fig. 5) was created by dividing the low by the high frequency data. The general central data has values of around 10, meaning the emissions in the low frequency data are approximately 10 times as bright as the GDIGS emissions in these areas. Fig. 6 shows uncertainty in the moment 0 ratio map.

The difference moment 1 map (Fig. 7) was made by subtracting the high from the low frequency data. Focusing again on the central area, the values are around 0 $km\ s^{-1}$, with light blue tinting not being statistically significant (Fig. 8). The velocity of the gas probed by GDIGS and GDIGS-Low is therefore about the same.

Lastly, the ratio FWHM map (Fig. 9) was made by dividing the low by the high frequency data, as with the moment 0 ratio map (Fig. 5). Central values are around 1, meaning that the lines at both frequencies have similar widths.

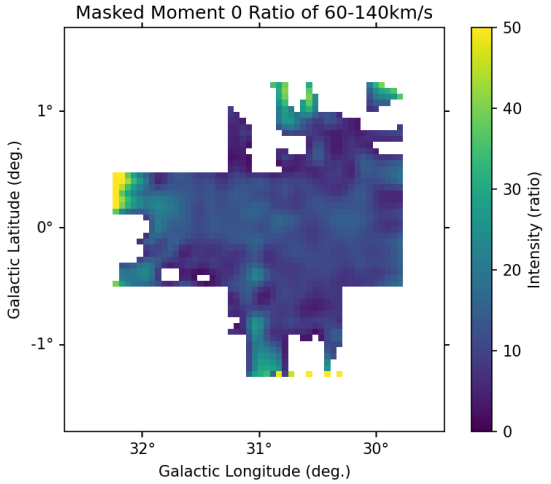

Figure 5. Moment 0 ratio map of GDIGS-Low data divided by GDIGS data.

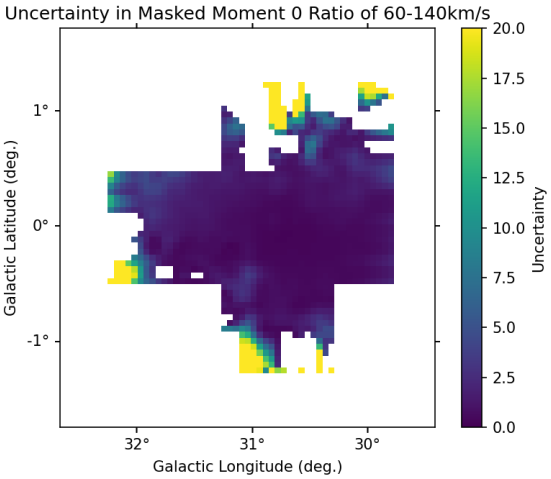

Figure 6. Uncertainty in moment 0 ratio map.

5. DENSITY ESTIMATES

To model the HRRL emission to create a density map of the W43 region, we assume a uniform density slab of ionized gas illuminated by a background source (see Shaver (1975) for details). We use a free-free spectrum for the background source and assume it is spatially uniform. The predictions from this model are then compared to the observed peak brightness ratio of the HRRLs.

Values range from about 10 to 30 e^{-} cm^{-3} in the general area corresponding to central regions on the comparison maps, but excluding the central dark artifact pattern (Figure 10). The values of the central regions, within the range of the color-bar, are less dense than estimated densities of HII regions, and more dense than expected densities of very low density diffuse gas (Luong et al. 2011). The variations seen in the region around 30°30' longitude and -0°20' latitude point to larger variations of densities within the diffuse ionized gas itself,

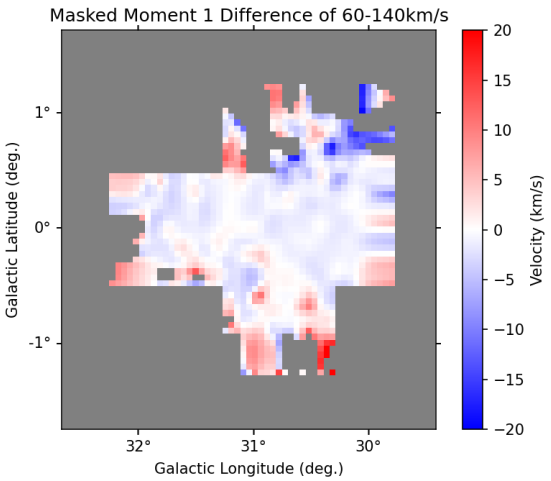

Figure 7. Moment 1 difference map of GDIGS data subtracted from GDIGS-Low data.

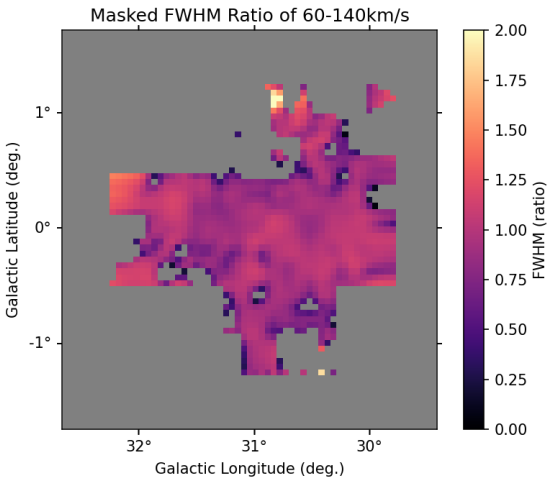

Figure 9. Moment 1 difference map of GDIGS data subtracted from GDIGS-Low data.

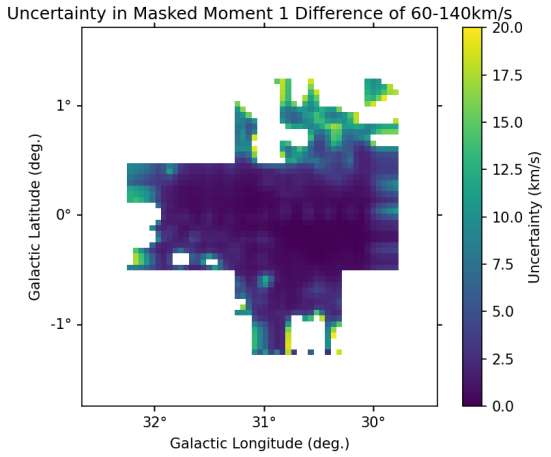

Figure 8. Uncertainty in moment 1 difference map.

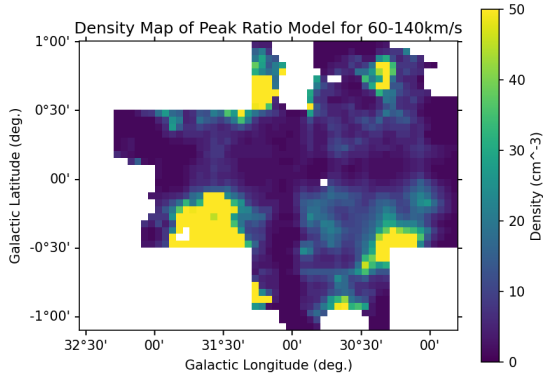

Figure 10. Density map modeled by comparing emission peaks of GDIGS-Low to GDIGS data.

possibly giving more context on the ionization of the gas.

However, the model and data used are limited. In Figure 10, there is a clear artifact pattern where observations overlapped, and there are areas of extremely high densities, notably around 31°30' longitude and -0°25' latitude with densities of upwards of 1,000 e^- cm^{-3}. For the model, we assumed that the ionized gas is of uniform density and that the background source is spatially uniform, which is not always a good approximation, as we know that the free-free emission changes on scales of arcminutes (see e.g., Emig et al. (2022)). Comparing the model to HRRL peak brightness ratio is also a second approach taken to mitigate the extreme density regions, as we first compared the model to the integrated intensity (moment 0) ratio. This was done in part as there was an absorption feature around 40 $km\ s^{-1}$ in the spectra of the cube that was affecting the moment 0 ratio, and using peak brightness instead largely avoided this issue.

6. CARBON EMISSIONS

Figure 11 shows a comparison of spectra between GDIGS and GDIGS-Low. We line up the peaks and continuum to allow for a strict comparison of line shapes. Hydrogen, helium, and carbon RRLs emissions are marked by the dotted green lines and labeled. Carbon is known to have a velocity offset of approximately 150 $km\ s^{-1}$ from hydrogen (Emig, K. L. et al. 2019). The emission around -150 $km\ s^{-1}$ is associated with local carbon.

Carbon is a useful probe of cold neutral gas, as its emission is highly dependent on temperature (brighter towards lower temperature regions), and it traces regions where carbon is ionized but hydrogen is in atomic or molecular form. This makes carbon RRLs (CRRLs) a unique probe of the atomic to molecular transition in

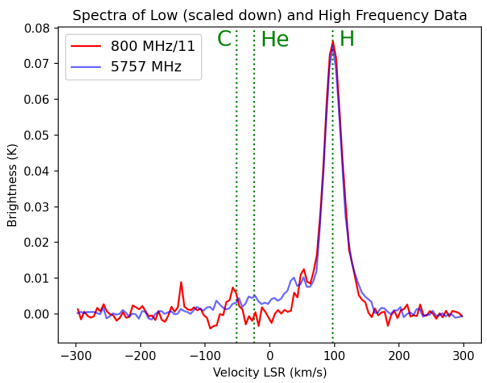

Figure 11. A comparison of spectra between GDIGS (blue) and GDIGS-Low (red), where GDIGS-Low has been scaled down by a factor of 11 to make it more visually comparable.

the ISM. CRRLs can therefore be an important factor in understanding how molecular clouds form. They were not detected in the GDIGS data, further limiting how precisely we can model the gas. When the GDIGS-Low survey is complete, we can potentially perform a systematic study of the properties of this gas with the aim of understanding the HI/H_2 interface.

7. CONCLUSIONS

Using GDIGS and GDIGS-Low RRL data from the GBT, we study the physical conditions of the diffuse ionized gas around the W43 star-forming region. We compute moment maps and comparisons thereof. We model HRRL emissions to make a density map, which, although limited by the model itself, shows variations in density within the gas that could provide information on how stellar feedback affects the ionization of the DIG. The detection of CRRLs in GDIGS-Low can be used to study molecular clouds. Similar analyses can be expected for the rest of the GDIGS-Low survey.

We thank Dr. Will Armentrout and Brenne Gregory for supporting this project, as well V. Catlett for assisting with coding. CK also thanks Dr. Loren Anderson, Dr. Kim Emig, and Riley Owens for encouraging their work, as well as Pedro Salas for being a great mentor.

Facilities: Green Bank Observatory

Software: Astropy (Astropy Collaboration et al. 2013, 2018, 2022), Matplotlib (Hunter 2007), Numpy (Harris et al. 2020), Reproject, SpectralCube (Ginsburg et al. 2019)

REFERENCES

Anderson, L. D., Luisi, M., Liu, B., et al. 2021, The Astrophysical Journal Supplement Series, 254, 28, doi: 10.3847/1538-4365/abef65

Astropy Collaboration, Robitaille, T. P., Tollerud, E. J., et al. 2013, A&A, 558, A33, doi: 10.1051/0004-6361/201322068

Astropy Collaboration, Price-Whelan, A. M., Sipőcz, B. M., et al. 2018, AJ, 156, 123, doi: 10.3847/1538-3881/aabc4f

Astropy Collaboration, Price-Whelan, A. M., Lim, P. L., et al. 2022, apj, 935, 167, doi: 10.3847/1538-4357/ac7c74

Emig, K. L., Salas, P., de Gasperin, F., et al. 2020, Astronomy & Astrophysics, 634, A138, doi: 10.1051/0004-6361/201936562

Emig, K. L., White, G. J., Salas, P., et al. 2022, Astronomy & Astrophysics, 664, A88, doi: 10.1051/0004-6361/202142596

Emig, K. L., Salas, P., de Gasperin, F., et al. 2019, A&A, 622, A7, doi: 10.1051/0004-6361/201834052

Ginsburg, A., Koch, E., Robitaille, T., et al. 2019, radio-astro-tools/spectral-cube: v0.4.4, v0.4.4, Zenodo, Zenodo, doi: 10.5281/zenodo.2573901

Harris, C. R., Millman, K. J., van der Walt, S. J., et al. 2020, Nature, 585, 357, doi: 10.1038/s41586-020-2649-2

Hunter, J. D. 2007, Computing in Science & Engineering, 9, 90, doi: 10.1109/MCSE.2007.55

Luisi, M., Anderson, L. D., Liu, B., et al. 2020, The Astrophysical Journal, 889, 96, doi: 10.3847/1538-4357/ab643e

Luong, Q. N., Motte, F., Schuller, F., et al. 2011, Astronomy & Astrophysics, 529, A41, doi: 10.1051/0004-6361/201016271

Motte, F., Schilke, P., & Lis, D. C. 2003, The Astrophysical Journal, 582, 277, doi: 10.1086/344538

Shaver, P. A. 1975, Pramana, 5, 1, doi: 10.1007/BF02875147